Science Advances
AAAS

advances.sciencemag.org/cgi/content/full/7/4/eaba5749/DC1

Supplementary Materials for

Possible detection of hydrazine on Saturn's moon Rhea

Mark Elowitz*, Bhalamurugan Sivaraman*, Amanda Hendrix, Jen-Iu Lo, Sheng-Lung Chou, Bing-Ming Cheng, B. N. Raja Sekhar, Nigel J. Mason

*Corresponding author. Email: elowitzr@earthlink.net (M.E.); bhala@prl.res.in (B.S.)

Published 22 January 2021, *Sci. Adv.* **7**, eaba5749 (2021)
DOI: 10.1126/sciadv.aba5749

This PDF file includes:

Supplementary Materials

Hapke Spectral Modelling

Model spectra of ice mixtures were derived based on computing the bi-directional reflectance using Hapke's equation. For each measured laboratory spectrum, the absorption coefficient is calculated given the measured absorbance and path length through the ice sample:

$$\alpha = \left[\frac{A}{\ln(10.)} \right] / d$$

where *A* is the measured absorbance and *d* is the photon path length. Using the absorption coefficient and water-ice grain size (derived from derivative spectroscopy of UVIS spectra), the internal transmission in the ice grain is calculated using the following expression:

$$\tau_i = \exp\left(-\frac{2a\alpha}{3} \right)$$

where α is the absorption coefficient and *a* is the size of the ice grain. The internal transmission coefficient is defined as the total fraction of radiation that enters a single ice grain and reaches another surface for the duration of one transit. Assuming a value for the optical constant, *n*, of water ice (the dominant component of the measured laboratory ice mixture) *(39)* and using the calculated absorption coefficient, the optical constant *k* is found from the following expression:

$$k = \frac{\alpha\lambda}{4\pi}$$

where λ is the wavelength of the radiation incident on the ice sample. Using the optical constants (*n*, *k*), the internal and external scattering coefficients are calculated using the following two approximations:

$$s_i = 1 - \frac{4}{n(n+1)^2}, \quad s_e = \frac{(n-1)^2 + k^2}{(n+1)^2 + k^2} + 0.05$$

These scattering coefficients are then used to calculate the wavelength-dependent single-scattering albedo of the ice grain. It is dependent on the chemical composition and grain size of the ice "regolith" on icy satellites, and can be expressed as *(40)*.

$$w = s_e + (1 - s_e)\frac{(1 - s_i)\tau_i}{1 - s_i\tau_i}$$

The ratio between scattering and absorption in the total extinction of the ice layer and is governed by the single-scattering albedo. In other words, the single-scattering albedo is the ratio of the scattering coefficient to the extinction coefficient.

The single-scattering albedo is then used in the Hapke equation to compute the bi-directional reflectance for each model spectrum.

$$R(i,e,g) = \frac{w}{4\pi}\frac{\mu_0}{\mu_0+\mu}\left[\left(1+B(\phi)\right)p(\phi)+M(\mu_0,\mu)\right]S\left(i,e,\phi,\bar{\theta}\right)$$

In the Hapke model equation, *w* is the single-scattering albedo, μ and μ_0 are the cosines of the emission and incident angles, $p(\phi)$ is the single grain phase function (for phase angle ϕ), $B(\phi)$ is the opposite effect parameter, $M(\mu_0,\mu)$ is the contribution from multiple scattering among ice grains and $S\left(i,e,\phi,\bar{\theta}\right)$ is the contribution from roughness at scales less than the spatial resolution of the detector. Therefore, *S* is a measure of macroscopic roughness. The roughness parameter represents the mean slope angle within a single pixel. It can be thought of as a microscale roughness parameter, from the grain size to a few millimetres. Thus, the roughness parameter will depend on the ice grain organization. The phase function, $p(\phi)$ depends on the asymmetry parameter, *b* and the backscattering fraction, *c*. The two-parameter (*b* and *c*) Henyey-Greenstein phase function for single grains is commonly used in the planetary science community *(40)*.

$$p(\alpha) = \frac{1+c}{2}\frac{1-b^2}{\left(1+2b\cos\phi+b^2\right)^{3/2}} + \frac{1-c}{2}\frac{1-b^2}{\left(1-2b\cos\phi+b^2\right)^{3/2}}$$

The behaviour of the phase function will therefore depend on the shape of the ice grains, their composition and internal structure. The single-scattering albedo, ω, depends on the size and microstructure of ice grains, as well as the particle composition and is the only wavelength-dependent Hapke parameter used in modelling spectra.

To determine the size of the ice grain particles used for input into the spectral models, first-derivative spectra were computed. The derivative measures the rate of change of absorbance with wavelength and is expressed by the following equation:

$$\left.\frac{ds}{d\lambda}\right|_i \approx \frac{s(\lambda_i)-s(\lambda_j)}{\Delta\lambda},\quad \Delta\lambda = \lambda_j-\lambda_i\ \ (\lambda_j>\lambda_i)$$

where $s(\lambda_i)$ and $s(\lambda_j)$ are two different spectral pixels. The first-derivatives of the UVIS spectra of Rhea were calculated using a three-point (quadratic) Lagrangian interpolation method. A smoothing kernel was applied to the UVIS data before applying the derivative to reduce any amplification in the noise that occurs when taking derivatives of spectra.

To determine the size of the ice grain particles used for input into the spectral models, first-derivative spectra were computed. The derivative measures the rate of change of absorbance with wavelength and is expressed by the following equation:

$$\left.\frac{ds}{d\lambda}\right|_i \approx \frac{s(\lambda_i)-s(\lambda_j)}{\Delta\lambda},\quad \Delta\lambda = \lambda_j-\lambda_i\ \ (\lambda_j>\lambda_i)$$

where $s(\lambda_i)$ and $s(\lambda_j)$ are two different spectral pixels. The first-derivatives of the UVIS spectra of Rhea were calculated using a three-point (quadratic) Lagrangian interpolation method. A smoothing kernel was applied to the UVIS data before applying the derivative to reduce any amplification in the noise that occurs when taking derivatives of spectra.

The location of the first-derivative peak in *wavelength space* determines the position of the water ice absorption edge seen in far-UV spectra of icy satellites. First-derivative analysis of modelled spectra of water-ice illustrates the change in the amplitude of the derivative peak and its wavelength as the size of the water-ice grain size changes. Differences in the water ice grain sizes and impurities will tend to produce shifts (Figure S1) in the position of the H_2O ice absorption edge *(15)* (Figure S1). In Figure S1, the steep spectral slope of the 165-nm absorption edge of water ice shifts to longer wavelengths as the size of the ice grains increases (left hand side of Figure S1). This is reflected in the position and amplitude of the derivative peak (right hand side of Figure S1). The derivative peak of several UVIS observations sampled from Rhea's leading and trailing hemispheres were compared with the modelled derivative peak shown on the right hand side of Figure S1. The black dashed line indicates the nominal position of the 165 nm absorption edge of pure water-ice and the red dashed line represents the location of the derivative peak of the average of the UVIS first-derivative spectra. The shift of the derivative peak towards longer wavelengths with respect to the nominal 165 nm location of pure water-ice indicates large grain sizes and/or possible non-water ice contaminants in the surface ice on Rhea. The results from the derivative analysis indicate an average grain diameter of about 3 microns for Rhea, with a range in grain sizes from 1 to 5 microns.

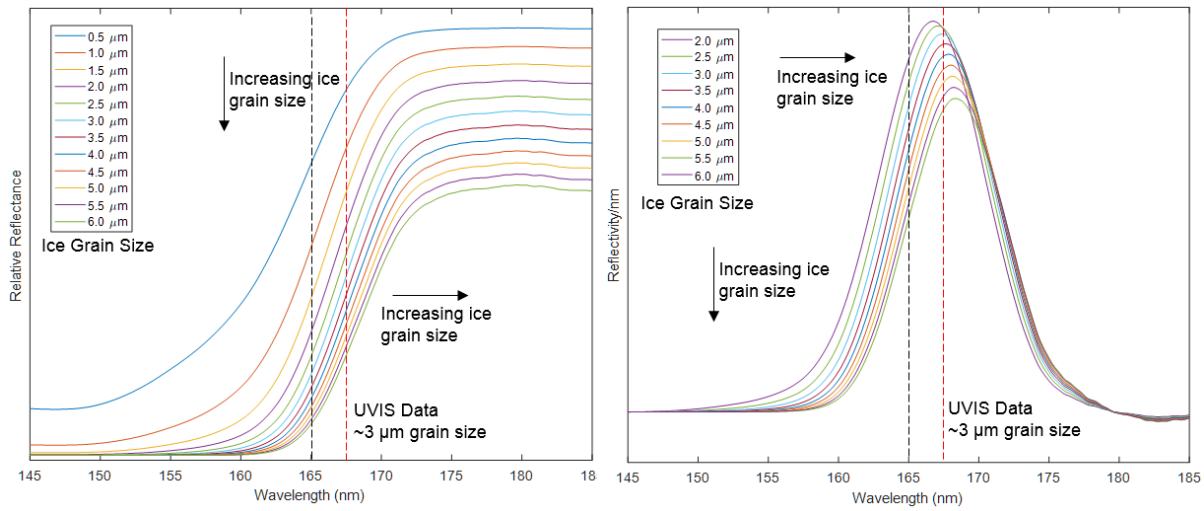

Figure S1: Illustration showing the behaviour of the first-derivative of the modelled far-UV absorption edge of water-ice. Note the shift of the peak of the derivative to longer wavelengths as the grain size increases. The amplitude of the derivative peak decreases as the modelled grain size increases (i.e. absorption increases or reflectivity decreases). The 3 μm grain size represents the average of the shift in the derivative peak from the nominal 165-nm position for the UVIS data used in producing modelled spectra.

Table S1: List of the molecular ices for which the VUV spectra are recorded at astrochemical icy conditions. The molecules that matched the FUV spectra of Rhea are highlighted in green. The data repository for the experimental data can be found at the AstroChemical Ices Database (ACID), link: www.prl.res.in/~dinesh/acid.

Acetaldehyde (CH_3CHO)
Acetonitrile (CH_3CN)
Acetylene (C_2H_2)
Adamantane ($C_{10}H_{16}$)
Aminoacetonitrile ($C_2H_4N_2$)
Ammonia (NH_3)
Ammonia + Carbon dioxide (NH_3+CO_2)
Ammonia + Oxygen (NH_3+O_2)
Ammonia + Water (NH_3+H_2O)
Ammonium hydroxide (NH_4OH)
Benzaldehyde (C_6H_5CHO)
Benzene (C_6H_6)
Benzene + Water
Benzonitrile(C_6H_5CN)
Benzyl alcohol ($C_6H_5CH_2OH$)
Benzyl amine ($C_6H_5CH_2NH_2$)
Butyronitrile ($CH_3CH_2CH_2CN$)
Carbon Dioxide (CO_2)
Carbon Disulpfide (CS_2)
Carbon Monoxide (CO)
Carbon Tetrachloride (CCl_4)
Carbonic Acid (H_2CO_3)
Carbonyl sulfide (OCS)
Chloroform ($CHCl_3$)
Cyclo-hexane (C_6H_{12})
Deuterium Chloride (DCl)
Dichloromethane (CH_2Cl_2)
Diethyl carbonate ($C_2H_5OCOOC_2H_5$)
Diethyl Ether ($(C_2H_5)_2O$)
Dimethyl carbonate ($CH_3OCOOCH_3$)

Dimethyl Ether (CH_3OCH_3)
Dimethyl Sulfoxide ($(CH_3)_2SO$)
Ethane (C_2H_6)
Ethanethiol (CH_3CH_2SH)
Ethanol(CH_3CH_2OH)
Ethanolamine (CH_2OH-CH_2NH_2)
Ethyl Acetate ($C_4H_8O_2$)
Ethyl Formate ($HCOOC_2H_5$)
Ethylene (C_2H_4)
Ethylene glycol ($CH_2OH)_2$
Formaldehyde (CH_2O)
Formamide (NH_2CHO)
Formic Acid (HCOOH)
Freon (CCl_2F_2)
Glycerol ($C_3H_8O_3$)
Hexane (C_6H_{14})
Hydrazine ($N_2H_4.H_2O$) (in monohydrate form)
Hydrogen Cyanide (HCN)
Hydrogen Peroxide + Water (H_2O_2+H_2O)
Isobutyronitrile ($(CH_3)_2CHCN$
Isoprene ($CH_2C_2HCH_2$)
Isopropyl alcohol ($CH_3CHOHCH_3$)
Methane (CH_4)
Methanethiol (CH_3SH)
Methanol (CH_3OH)
Methyl acetate (CH_3COOCH_3)
Methyl Chloroformate ($C_2H_3ClO_2$)
Methyl formate (CH_3CO_2H)
Nitric oxide (NO)
Nitrobenzene ($C_6H_5NO_2$)

Nitrogen dioxide (NO_2)
Nitrous Oxide (N_2O)
Organic residue (PAH from benzene irradiation)
Oxygen (O_2)
Ozone (O_3)
Pentanethiol ($CH_3(CH_2)_4SH$)
Phenyl acetate ($C_6H_5COOCH_3$)
Phenyl isocyanate (C_6H_5NCO)
Pluto Mixture (N_2 + CO + CH_4)
Propanethiol ($CH_3CH_2CH_2SH$)
Propargyl Alcohol (C_3H_4O)
Propargyl ether ($C_3H_3OC_3H_3$)
Propionic acid ($CH_3CH_2CO_2H$)
Propionitrile (CH_3CH_2CN)
Propyne (C_3H_4)
Pyridine (C_5H_5N)
Pyrrole (C_4H_4NH)
Silane (SiD_4)
Styrene ($C_6H_5CHCH_2$)
Sulphur dioxide (SO_2)
Tetrahydrofuran ($(CD_2)_4O$)
Thioanisole ($CH_3SC_6H_5$)
Thionylchloride ($SOCl_2$)
Thiophene (C_4H_4S)
Toulene $C_6H_5CH_3$
Trichloroethylene (C_2HCl_3)
Trichloroethylene ($ClCH{=}CCl_2$)
Water (H_2O)
Xylene ($C_6H_4(CH_3)_2$)
α, β – Pinene, Limonene ($C_{10}H_{16}$)

REFERENCES AND NOTES

1. J. M. Moore, P. M. Schenk, in *Lunar and Planetary Science Conference XXXVIII* (2007).

2. R. J. Wagner, G. Neukum, B. Giese, T. Roatsch, U. Wolf, in *Lunar and Planetary Science Conference XXXVIII* (2007).

3. C. J. A. Howett, J. R. Spencer, J. Pearl, M. Segura, Thermal inertia and bolometric Bond albedo values for Mimas, Enceladus, Tethys, Dione, Rhea and Iapetus as derived from Cassini/CIRS measurements. *Icarus* **206**, 573–593 (2010).

4. A. Verbiscer, R. French, M. Shuwalter, P. Helfenstein, Enceladus: Cosmic graffiti artist caught in the Act. *Science* **315**, 815 (2007).

5. U. Fink, H. P. Larson, T. N. I. Gautier III, R. R. Treffers, Infrared spectra of the satellites of Saturn—Identification of water ice on Iapetus, Rhea, Dione, and Tethys. *Astrophys. J.* **207**, L63–L67 (1976).

6. A. R. Hendrix, T. A. Cassidy, G. M. Holsclaw, C. Paranicas, C. J. Hansen, in *EPSC-DPS Joint Meeting* (2011), vol. 6, pp. 1638.

7. A. R. Hendrix, G. Filacchione, C. Paranicas, P. Schenk, F. Scipioni, Icy Saturnian satellites: Disk-integrated UV-IR characteristics and links to exogenic processes. *Icarus* **300**, 103–114 (2018).

8. B. D. Teolis, J. H. White, Dione and Rhea seasonal exospheres revealed by Cassini CAPS and INMS. *Icarus* **272**, 277–289 (2016).

9. P. Schenk, D. P. Hamilton, R. E. Johnson, W. B. McKinnon, C. Paranicas, J. Schmidt, M. R. Showalter, Plasma, plumes and rings: Saturn system dynamics as recorded in global color patterns on its midsize icy satellites. *Icarus* **211**, 740–757 (2011).

10. A. J. Verbiscer, J. Veverka, Albedo dichotomy of Rhea: Hapke analysis of Voyager photometry. *Icarus* **82**, 336–353 (1989).

11. E. M. Royer, A. R. Hendrix, First far-ultraviolet disk-integrated phase curve analysis of Mimas, Tethys and Dione from the Cassini-UVIS data sets. *Icarus* **242**, 158–171 (2014).

12. G. Strazzulla, A. C. Castorina, M. E. Palumbo, Ion irradiation of astrophysical ices. *Planet. Space Sci.* **43**, 1247–1251 (1995).

13. P. A. Gorry, General least-squares smoothing and differentiation by the convolution (Savitzky-Golay) method. *Anal. Chem.* **62**, 570–573 (1990).

14. A. Savitzky, M. J. E. Golay, Smoothing and differentiation of data by simplified least squares procedures. *Anal. Chem.* **36**, 1627–1639 (1964).

15. A. R. Hendrix, C. J. Hansen, Ultraviolet observations of Phoebe from the Cassini UVIS. *Icarus* **193**, 323–333 (2008).

16. E. M. Royer, L. W. Esposito, J. P. Elliott, Mapping of the 185nm absorption feature on the icy satellites of Saturn, in *Lunar and Planetary Science Conference L*, (2019).

17. B. D. Teolis, G. H. Jones, P. F. Miles, R. L. Tokar, B. A. Magee, J. H. Waite, E. Roussos, D. T. Young, F. J. Crary, A. J. Coates, R. E. Johnson, W.-L. Tseng, R. A. Baragiola, Cassini finds an oxygen–carbon dioxide atmosphere at Saturn's icy Moon Rhea. *Science* **330**, 1813–1815 (2010).

18. B. Buratti, J. Veverka, Voyager photometry of Rhea, Dione, Tethys, Enceladus and Mimas. *Icarus* **58**, 254–264 (1984).

19. C. J. A. Howett, J. R. Spencer, T. Hurford, A. Verbiscer, M. Segura, Thermophysical property variations across Dione and Rhea. *Icarus* **241**, 239–247 (2014).

20. F. Postberg, S. Kempf, J. Schmidt, N. Brilliantov, A. Beinsen, B. Abel, U. Buck, R. Srama, Sodium salts in E-ring ice grains from an ocean below the surface of Enceladus. *Nature* **459**, 1098–1101 (2009).

21. H. Hussmann, F. Sohl, T. Spohn, Subsurface oceans and deep interiors of medium-sized outer planet satellites and large trans-neptunian objects. *Icarus* **185**, 258–273 (2006).

22. T. T. Koskinen, R. V. Yelle, D. S. Snowden, P. Lavvas, B. R. Sandel, F. J. Capalbo, Y. Benilan, R. A. West, The mesosphere and lower thermosphere of Titan revealed by Cassini/UVIS stellar occultations. *Icarus* **216**, 507–534 (2011).

23. M. J. Loeffler, U. Raut, R. A. Baragiola, Radiation chemistry in ammonia-water ices. *J. Chem. Phys.* **132**, 054508 (2010).

24. W. Zheng, D. Jewitt, Y. Osamura, R. I. Kaiser, Formation of nitrogen and hydrogen-bearing molecules in solid ammonia and implications for solar system and interstellar ices. *Astrophys. J.* **674**, 1242–1250 (2008).

25. V. De La Haye, J. H. Waite Jr., R. E. Johnson, R. V. Yelle, T. E. Cravens, J. G. Luhmann, W. T. Kasprzak, D. A. Gell, B. Magee, F. Leblanc, M. Michael, S. Jurac, I. P. Robertson, Cassini ion and neutral mass spectrometer data in Titan's upper atmosphere and exosphere: Observation of a suprathermal corona. *J. Geophys. Res. Space Physics* **112**, A07309 (2007).

26. N. J. Mason, A. Dawes, P. D. Holtom, R. J. Mukerji, M. P. Davis, B. Sivaraman, R. I. Kaiser, S. V. Hoffmann, D. A. Shaw, VUV spectroscopy and photo-processing of astrochemical ices: An experimental study. *Faraday Discuss.* **133**, 311–329 (2006).

27. L. W. Esposito, C. A. Barth, J. E. Colwell, G. M. Lawrence, W. E. McClintock, A. I. F. Stewart, H. U. Keller, A. Korth, H. Lauche, M. C. Festou, A. L. Lane, C. J. Hansen, J. N. Maki, R. A. West, H. Jahn, R. Reulke, K. Warlich, D. E. Shemansky, Y. L. Yung, The Cassini Ultraviolet Imaging Spectrograph Investigation. *Space Sci. Rev.* **115**, 299–361 (2004).

28. W. E. McClintock, G. J. Rottman, T. N. Woods, Paper presented at the Proceedings—SPIE The International Society for Optical Engneering, 2000.

29. R. G. Bhuin, B. Sivaraman, J.-I. Lo, B. N. R. Sekhar, B.-M. Cheng, T. Pradeep, N. J. Mason, Communication: Vacuum ultraviolet photoabsorption of interstellar icy thiols. *J. Chem. Phys.* **141**, 231101 (2014).

30. G. A. Cruz-Diaz, G. M. M. Caro, Y.-J. Chen, Vacuum-UV absorption spectroscopy of interstellar ice analogues. III. Isotopic effects. *Mon. Notices R. Astron. Soc.* **439**, 2370–2376 (2014).

31. A. Dawes, R. J. Mukerji, M. P. Davis, P. D. Holtom, S. M. Webb, B. Sivaraman, S. V. Hoffmann, D. A. Shaw, N. J. Mason, Morphological study into the temperature dependence of solid ammonia under astrochemical conditions using vacuum ultraviolet and Fourier-transform infrared spectroscopy. *J. Chem. Phys.* **126**, 244711 (2007).

32. A. Dawes, N. Pascual, S. V. Hoffmann, N. C. Jones, N. J. Mason, Vacuum ultraviolet photoabsorption spectroscopy of crystalline and amorphous benzene. *Phys. Chem. Chem. Phys.* **19**, 27544–27555 (2017).

33. A. Dawes, N. Pascual, N. J. Mason, S. Gärtner, S. V. Hoffmann, N. C. Jones, Probing the interaction between solid benzene and water using vacuum ultraviolet and infrared spectroscopy. *Phys. Chem. Chem. Phys.* **20**, 15273–15287 (2018).

34. S. Pavithraa, J.-I. Lo, K. Rahul, B. N. Raja Sekhar, B.-M. Cheng, N. J. Mason, B. Sivaraman, Vacuum ultraviolet photoabsorption of prime ice analogues of Pluto and Charon. *Spectrochim. Acta A Mol. Biomol. Spectrosc.* **190**, 172–176 (2018).

35. S. Pavithraa, D. Sahu, G. Seth, J.-I. Lo, B. N. Raja Sekhar, B.-M. Cheng, A. Das, N. J. Mason, B. Sivaraman, SH stretching vibration of propanethiol ice—A signature for its identification in the interstellar icy mantles. *Astrophys. Space Sci.* **362**, 126 (2017).

36. B. Sivaraman, B. G. Nair, B. N. Raja Sekhar, J.-I. Lo, R. Sridharan, B.-M. Cheng, N. J. Mason, Vacuum ultraviolet photoabsorption of pure solid ozone and its implication on the identification of ozone on Moon. *Chem. Phys. Lett.* **603**, 33–36 (2014).

37. B. Sivaraman, S. Pavithraa, J.-I. Lo, B. N. R. Sekhar, H. Hill, B.-M. Cheng, N. J. Mason, Vacuum ultraviolet photoabsorption spectra of nitrile ices for their identification on Pluto. *Astrophys. J.* **825**, 141 (2016).

38. B. Sivaraman, B. N. Raja Sekhar, N. C. Jones, S. V. Hoffmann, N. J. Mason, VUV spectroscopy of formamide ices. *Chem. Phys. Lett.* **554**, 57–59 (2012).

39. S. G. Warren, Optical constants of ice from the ultraviolet to the microwave. *Appl. Optics* **23**, 1206–1225 (1984).

40. B. Hapke, *Theory of Reflectance and Emittance Spectroscopy* (Cambridge Univ. Press, ed. 2, 2012).